Eur. Phys. J. C (2024) 84:820
https://doi.org/10.1140/epjc/s10052-024-13056-2

THE EUROPEAN PHYSICAL JOURNAL C

Check for updates

Regular Article - Experimental Physics

K_S^0 meson production in inelastic p+p interactions at 31, 40 and 80 GeV/c beam momentum measured by NA61/SHINE at the CERN SPS

NA61/SHINE Collaboration

N. Abgrall[29], H. Adhikary[13], P. Adrich[15], K. K. Allison[26], N. Amin[5], E. V. Andronov[22], T. Antićić[3], I.-C. Arsene[12], M. Bajda[16], Y. Balkova[18], M. Baszczyk[17], D. Battaglia[25], A. Bazgir[13], S. Bhosale[14], M. Bielewicz[15], A. Blondel[4], M. Bogomilov[2], Y. Bondar[13], N. Bostan[25], A. Brandin[22], A. Bravar[29], W. Bryliński[21], J. Brzychczyk[16], M. Buryakov[22], A. F. Camino[28], M. Ćirković[23,a], M. Csanád[8], J. Cybowska[21], T. Czopowicz[13], C. Dalmazzone[4], N. Davis[14], A. Dmitriev[22], P. von Doetinchem[27], W. Dominik[19], P. Dorosz[17], J. Dumarchez[4], R. Engel[5], G. A. Feofilov[22], L. Fields[25], Z. Fodor[7,20], M. Friend[9], M. Gaździcki[6,13], O. Golosov[22], V. Golovatyuk[22], M. Golubeva[22], K. Grebieszkow[21], F. Guber[22], A. Haesler[29], S. N. Igolkin[22], S. Ilieva[2], A. Ivashkin[22], A. Izvestnyy[22], K. Kadija[3], N. Kargin[22], N. Karpushkin[22], E. Kashirin[22], M. Kiełbowicz[14], V. A. Kireyeu[22], H. Kitagawa[10], R. Kolesnikov[22], D. Kolev[2], A. Korzenev[29], Y. Koshio[10], V. N. Kovalenko[22], S. Kowalski[18], B. Kozłowski[21], A. Krasnoperov[22], W. Kucewicz[17], M. Kuchowicz[20], M. Kuich[19], A. Kurepin[22], A. László[7], M. Lewicki[20], G. Lykasov[22], V. V. Lyubushkin[22], M. Maćkowiak-Pawłowska[21], Z. Majka[16], A. Makhnev[22], B. Maksiak[15], A. I. Malakhov[22], A. Marcinek[14], A. D. Marino[26], H.-J. Mathes[5], T. Matulewicz[19], V. Matveev[22], G. L. Melkumov[22], A. Merzlaya[12], Ł. Mik[17], A. Morawiec[16], S. Morozov[22], Y. Nagai[8], T. Nakadaira[9], M. Naskręt[20], S. Nishimori[9], V. Ozvenchuk[14], O. Panova[13], V. Paolone[28], O. Petukhov[22], I. Pidhurskyi[6,13], R. Płaneta[16], P. Podlaski[19], B. A. Popov[22,4], B. Pórfy[7,8], M. Posiadała-Zezula[19], D. S. Prokhorova[22], D. Pszczel[15], S. Puławski[18], J. Puzović[23†], R. Renfordt[18], L. Ren[26], V. Z. Reyna Ortiz[13], D. Röhrich[11], E. Rondio[15], M. Roth[5], Ł. Rozpłochowski[14], B. T. Rumberger[26], M. Rumyantsev[22], A. Rustamov[1,6], M. Rybczynski[13], A. Rybicki[14], K. Sakashita[9], K. Schmidt[18], A. Yu. Seryakov[22], P. Seyboth[13], U. A. Shah[13], Y. Shiraishi[10], A. Shukla[27], M. Słodkowski[21], P. Staszel[16], G. Stefanek[13], J. Stepaniak[15], M. Strikhanov[22], H. Ströbele[6], T. Šuša[3], L. Swiderski[15], J. Szewiński[15], R. Szukiewicz[20], A. Taranenko[22], A. Tefelska[21], D. Tefelski[21], V. Tereshchenko[22], A. Toia[6], R. Tsenov[2], L. Turko[20], T. S. Tveter[12], M. Unger[5], M. Urbaniak[18], F. F. Valiev[22], D. Veberič[5], V. V. Vechernin[22], V. Volkov[22], A. Wickremasinghe[24], K. Wójcik[18], O. Wyszyński[13], A. Zaitsev[22], E. D. Zimmerman[26], A. Zviagina[22], R. Zwaska[24]

[1] National Nuclear Research Center, Baku, Azerbaijan
[2] Faculty of Physics, University of Sofia, Sofia, Bulgaria
[3] Ruđer Bošković Institute, Zagreb, Croatia
[4] LPNHE, University of Paris VI and VII, Paris, France
[5] Karlsruhe Institute of Technology, Karlsruhe, Germany
[6] University of Frankfurt, Frankfurt, Germany
[7] Wigner Research Centre for Physics, Budapest, Hungary
[8] Eötvös Loránd University, Budapest, Hungary
[9] Institute for Particle and Nuclear Studies, Tsukuba, Japan
[10] Okayama University, Okayama, Japan
[11] University of Bergen, Bergen, Norway
[12] University of Oslo, Oslo, Norway
[13] Jan Kochanowski University, Kielce, Poland
[14] Institute of Nuclear Physics, Polish Academy of Sciences, Kraków, Poland
[15] National Centre for Nuclear Research, Warsaw, Poland
[16] Jagiellonian University, Kraków, Poland
[17] AGH-University of Science and Technology, Kraków, Poland
[18] University of Silesia, Katowice, Poland
[19] University of Warsaw, Warsaw, Poland
[20] University of Wrocław, Wrocław, Poland

Published online: 15 August 2024

[21] Warsaw University of Technology, Warsaw, Poland
[22] Affiliated with an institution covered by a cooperation agreement with CERN, Geneva, Switzerland
[23] University of Belgrade, Belgrade, Serbia
[24] Fermilab, Batavia, USA
[25] University of Notre Dame, Notre Dame, USA
[26] University of Colorado, Boulder, USA
[27] University of Hawaii at Manoa, Honolulu, USA
[28] University of Pittsburgh, Pittsburgh, USA
[29] University of Geneva, Geneva, Switzerland
† Deceased

Received: 1 March 2024 / Accepted: 17 June 2024

Abstract The yields of K^0_S mesons have been measured in inelastic p+p interactions at incident projectile momenta of 31, 40 and 80 GeV/c ($\sqrt{s_{NN}} = 7.7, 8.8$ and 12.3 GeV, respectively). The data were recorded by the NA61/SHINE spectrometer at the CERN Super Proton Synchrotron and the K^0_S mesons identified via their decays into $\pi^+\pi^-$ pairs. Double-differential distributions are presented as function of transverse momentum and rapidity. The mean multiplicities of K^0_S mesons were determined to be $(5.95 \pm 0.19(stat) \pm 0.30(sys)) \times 10^{-2}$ at 31 GeV/c, $(7.61 \pm 0.13(stat) \pm 0.43(sys)) \times 10^{-2}$ at 40 GeV/c and $(11.58 \pm 0.12(stat) \pm 0.55(sys)) \times 10^{-2}$ at 80 GeV/c. The results on K^0_S production are compared with the production of charged kaons in corresponding reactions and with model calculations (Epos1.99, SMASH 2.0 and PHSD) as well as with published data from other experiments.

Contents

No affiliated with NA61/SHINE is not connected with University of Geneva.

[a] e-mail: marjan.cirkovic@cern.ch (corresponding author)

1 Introduction

The measurement of hadron production in proton–proton interactions plays a key role in understanding nucleus–nucleus collisions. In particular, it can shed some light on the creation process of Quark Gluon Plasma (QGP) [1], on its properties, and on the characterization of the phase transition between hadronic matter and the QGP. One of the key signals of QGP creation is the enhanced production of s and $\bar{s}$ quarks, carried mostly by kaons [2]. The experimental results indicate that the creation of the QGP starts in nucleus–nucleus collisions at centre of mass energies from 10 to 20 GeV [3], which is the realm of the NA61/SHINE experiment at CERN. To explore this region systematically NA61/SHINE studies observables indicative of the QGP by a two-dimensional scan in collision energy and nuclear mass number of the colliding nuclei. The NA61/SHINE collaboration has collected data on charged and neutral (strange) particle production in p+p, p+Pb, Be+Be, Ar+Sc, Xe+La and Pb+Pb interactions in the beam momentum range from 13A to 158A GeV/c [4]. Neutral kaons are detected via the weak decay of K^0_S, which does not differentiate between K and $\bar{K}$ states. Their measurement allows to scrutinize the validity of isospin symmetry and of the strangeness enhancement observed in nuclear collisions. In this paper, we present the results of K^0_S production in p+p collisions at 31, 40, and 80 GeV/c. Results on neutral kaon spectra in p+p at 158 GeV/c can be found in Ref. [5]. Charged kaon spectra in p+p at 31, 40, 80 and 158 GeV/c are reported in Ref. [6]. These measurements of charged and neutral kaons constitute the basis for the interpretation of the results obtained in heavier systems collected by NA61/SHINE. Thanks to high statistics, large acceptance, and good momentum resolution, the results presented here have significantly higher precision than previously published measurements in the SPS energy range.

The paper is organised as follows. In Sect. 2 details of the NA61/SHINE detector system are presented. Section 3 is devoted to describing the analysis method. The results are shown in Sect. 4. In Sect. 5 they are compared to published world data and model calculations. Section 6 closes the paper with a summary and outlook.

The following units, variables and definitions are used in this paper. The particle mass and energy are presented in GeV, while particle momentum is shown in GeV/c. The particle rapidity y is calculated in the proton–proton collision center of mass system (cms), $y = 0.5 \cdot ln[(E + cp_L)/(E - cp_L)]$, where E and p_L are the particle energy and longitudinal momentum. The transverse component of the momentum is denoted as p_T. The momentum in the laboratory frame is denoted p_{lab} and the collision energy per nucleon pair in the centre of mass by $\sqrt{s_{NN}}$.

2 Experimental setup

The NA61/SHINE collaboration uses a large acceptance spectrometer located in the CERN North Area. The schematic layout of the NA61/SHINE detector during the $p+p$ data-taking is shown in Fig. 1. A detailed description of the experimental setup can be found in Ref. [7], while the details on the simulation in describing the detector performance across different kinematic variables as well as its inefficiencies can be found in Ref. [8].

The main components of the NA61/SHINE spectrometer are four large-volume Time Projection Chambers (TPCs). Two of them, the vertex TPCs (VTPC-1 and VTPC-2), are located in the magnetic fields of two super-conducting dipole magnets with a maximum combined bending power of 9 Tm, which corresponds to about 1.5 T and 1.1 T in the upstream and downstream magnets, respectively. This field strength was used for data taking at 158 GeV/c and scaled down in proportion to the lower beam momenta to obtain similar $y - p_T$ acceptance at all beam momenta. Two large main TPCs (MTPC-L and MTPC-R) and two walls of pixel Time-of-Flight (ToF-L/R) detectors are positioned symmetrically to the beamline downstream of the magnets. A GAP-TPC (GTPC) is placed between VTPC-1 and VTPC-2 directly on the beamline. It closes the gap between the beam axis and the sensitive volumes of the other TPCs. The TPCs are filled with Ar and CO_2 gas mixtures in proportions 90:10 for the VTPCs and 95:5 for the MTPCs. Particle identification in the TPCs is based on measurements of the specific energy loss ($\mathrm{d}E/\mathrm{d}x$) in the chamber gas. Typical values for the momentum resolution are $\sigma(p)/p^2 = 7 \times 10^{-4}$ (GeV/c)$^{-1}$ for low-momentum tracks measured only in VTPC-1 ($p \leq 8$ GeV/c) and 3×10^{-3} (GeV/c)$^{-1}$ for tracks traversing the full detector up to and including the MTPCs ($p \geq 8$ GeV/c).

Secondary beams of positively charged hadrons at momenta of 31, 40 and 80 GeV/c were used to collect the data for the analysis presented in this paper. These beams were produced from a 400 GeV/c proton beam extracted from the SPS in a slow extraction mode with a flat-top of 10 s. The beam momentum and intensity were adjusted by appropriate settings of the H2 beam line magnet currents and collimators. Protons from the secondary hadron beam are identified by two Cherenkov counters, C1 [10] and C2 (THC). The C1 counter, using a coincidence of six out of the eight photomultipliers placed radially along the Cherenkov ring, provides identification of protons, while the THC, operated at a pressure lower than the proton threshold, is used in anti-coincidence in the trigger logic. A selection based on the signals from the Cherenkov counters allowed to identify beam protons with a purity of about 99%, as demonstrated by a measurement of the specific ionization energy loss $\mathrm{d}E/\mathrm{d}x$ of the beam particles by bending the 31 GeV/c beam into

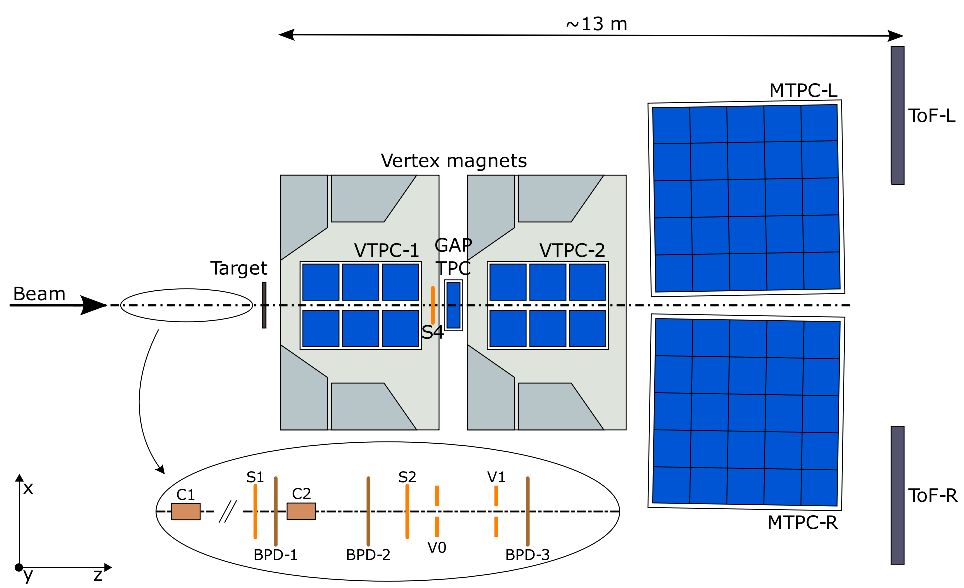

Fig. 1 The schematic layout of the NA61/SHINE experiment at the CERN SPS during $p+p$ data taking (horizontal cut, not to scale). The beam and trigger detector configuration used for data taking in 2009 is shown in the inset (see Refs. [7–9] for a detailed description). The chosen coordinate system is drawn on the lower left: its origin lies in the middle of the VTPC-2 on the beam axis

the TPCs using the full magnetic field strength [11]. A set of scintillation (S1, S2 and V0, V1) and beam position detectors (BPDs) upstream of the spectrometer provides timing reference, and position measurements of incoming beam particles.

$$\text{beam} \equiv \text{S1} \wedge \text{S2} \wedge \overline{\text{V0}} \wedge \overline{\text{V1}} \wedge \overline{\text{V1'}} \wedge \text{CEDAR} \wedge \overline{\text{THC}} \quad (1)$$

The trigger scintillation counter S4 placed downstream of the target has a diameter of 2 cm. It is used to trigger the readout whenever an incoming beam particle, which is registered upstream of the target, does not hit S4, which indicates that an interaction occurred in the target area.

$$\text{interaction} \equiv \text{beam} \wedge \overline{\text{S4}} \quad (2)$$

A cylindrical target vessel of 20.29 cm length and 3 cm diameter was placed upstream of the entrance window of VTPC-1 (center of the target is at z = -581 cm in the NA61/SHINE coordinate system). The vessel was filled with liquid hydrogen corresponding to an interaction length of 2.8%. The liquid hydrogen had a density of approximately 0.07 g/cm^3. Data were taken with the vessel filled with liquid hydrogen and being empty. Here, only events recorded with the target vessel filled with hydrogen were analyzed.

3 Analysis

3.1 Data sets

The presented results on K^0_S production in inelastic p+p interactions at $p_{beam} = 31, 40$ and 80 GeV/c are based on data recorded in 2009. Table 1 summarizes basic information about the data sets used in the analysis, the number of events selected by the interaction trigger, and the number of events after all selection criteria. The event numbers recorded with the interaction trigger were 2.85 M, 4.37 M and 3.80 M, respectively. The drop in event numbers after application of the selection criteria is caused mainly by BPD reconstruction inefficiencies and off-target interactions accepted by the trigger logic.

3.2 Analysis method

The event vertex and the produced particle tracks were reconstructed using the standard NA61/SHINE software. Details of the track and vertex reconstruction procedures can be found in Refs. [8,9,12]. Detector parameters were optimized by a data-based calibration procedure, which also considered their time dependence; for details, see Refs. [6,13]. The following section enumerates the criteria for selecting events, tracks and the K^0_S decay topology. Then the simulation-based correction procedure is described and used to quantify the losses due to reconstruction inefficiencies and limited geometrical acceptance.

3.3 Event selection

The criteria for selection of inelastic p+p interactions are the following:

(i) Interaction is recognized by the trigger logic defined in Eq. 2
(ii) Elimination of off-time interactions by rejecting all beam particles that passed through the S1 counter within $|\Delta t| < 2\,\mu$s of the interaction time that defined the event.
(iii) Beam particle trajectory was measured in at least three planes out of four of BPD-1 and BPD-2 and in both planes of BPD-3.
(iv) The presence of a reconstructed primary vertex in the event [14,15].
(v) The z position of the interaction vertex (fitted using the beam trajectory and TPC tracks) not farther away than 9 cm from the center of the target vessel.
(vi) Events with a single, well-measured, positively charged track with absolute momentum close to the beam momentum ($p > p_{beam} - 1$ GeV/c) were rejected.

The background due to elastic interactions was removed via selection criteria (iv) and (vi). The contribution from off-target interactions was reduced by selection criteria (v). Simulations corrected the losses of inelastic p+p interactions due to the event selection procedure. The corresponding correction factors are 1.46 ($p_{beam} = 31$ GeV/c), 1.45 ($p_{beam} = 40$ GeV/c) and 1.48 ($p_{beam} = 80$ GeV/c).

Table 1 Data sets used for the analysis of K^0_S production. The beam momentum is denoted by p_{beam}, whereas $\sqrt{s_{NN}}$ is the energy available in the center-of-mass system for the nucleon pair. The event selection criteria are described in Sect. 3.3

p_{beam} (GeV/c)	$\sqrt{s_{NN}}$ (GeV)	Number of recorded events with interaction trigger	Number of events after selection criteria
31	7.7	2.85×10^6	0.83×10^6
40	8.8	4.37×10^6	1.24×10^6
80	12.3	3.80×10^6	1.48×10^6

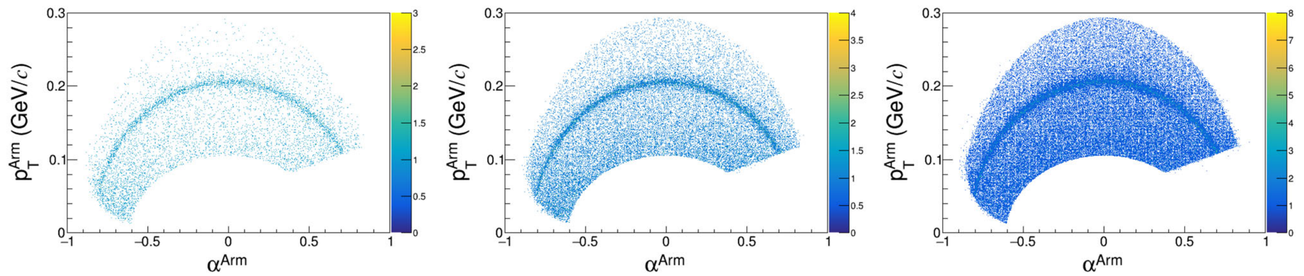

Fig. 2 Armenteros–Podolanski plots of V^0 candidates after all track and topology selection criteria for $p_{beam} = 31, 40$ and 80 GeV/c from left to right. The boundaries on the plots' left and right sides result from using the $cos\Theta^*$ selection criteria, while the upper and lower boundaries are shaped by selecting a certain invariant mass range

3.4 Track and topology selection

Neutral strange particles are detected and measured using their weak decay into charged particles. The K^0_S decays into $\pi^+ + \pi^-$ with a branching ratio of 69.2% [16]. The decay particles form the so-called V^0 topology. K^0_S decay candidates (V^0s) are obtained by pairing all positively with all negatively charged pion candidates. The tracks of the decay pions and the V^0 topology are subject to the following additional selection criteria:

(i) For each candidate track the minimum number of measured clusters in VTPC-1 and VTPC-2 must be 15.
(ii) All pion tracks must have a measured specific energy loss ($\mathrm{d}E/\mathrm{d}x$) in the TPCs within $\pm 3\sigma$ around the nominal Bethe-Bloch value for charged pions. σ represents the typical standard deviation of a Gaussian fitted to the $\mathrm{d}E/\mathrm{d}x$ distribution of pions. Since only small variations of σ were observed for different bins and beam momenta, a constant value $\sigma = 0.052$ is used [17]. This selection criterion applies only to experimental data, not MC-simulated events (see below).
(iii) The distance $|\Delta z|$ between the z-coordinates of the primary production and the K^0_S decay vertices is required to lie in the rapidity dependent range: $|\Delta z| > e^{a+b\cdot y_{lab}}$, with y_{lab} the rapidity in the laboratory and a and b constants which amount to 1.91 and 0.99 for the $p_{beam} =$ 31 GeV/c, 1.71 and 0.95 for $p_{beam} = 40$ GeV/c, and 1.85 and 0.90 for $p_{beam} = 80$ GeV/c data sets, respectively.
(iv) The distance between the track extrapolated to the interaction plane and the interaction point (impact parameter) must be smaller than 0.25 cm, with impact parameter given by $\sqrt{(b_x/2)^2 + {b_y}^2}$.
(v) The cosine of the angle between the V^0 and π^+ momentum vectors in the K^0_S rest frame has to be in the range: $-0.97 < cos\Theta^* < 0.85$.

The quality of the aforementioned track and topology selection criteria is illustrated in Fig. 2. The population of K^0_S decay candidates is shown as a function of the two Armenteros–Podolansky variables p_T^{Arm} and α^{Arm} [18] and after all track and topology selection criteria. The quantity p_T^{Arm} is the transverse momentum of the decay particles with respect to the direction of motion of the V^0 candidate and $\alpha^{Arm} = (p_L^+ - p_L^-)/(p_L^+ + p_L^-)$, where p_L^+ and p_L^- are the longitudinal momenta of the positively and negatively charged V^0 daughter particles, measured with respect to the V^0 direction of motion. On the plots (see Fig. 2) one can see that the contributions of Λ and $\bar{\Lambda}$ hyperons are removed by the topological selection criteria.

3.5 Raw K^0_S yields

The double differential uncorrected yields of K^0_S are determined by studying the invariant mass distributions of the accepted pion pairs in bins of rapidity and transverse momentum (examples are presented in Fig. 3). The K^0_S decays will appear as a peak over a smooth combinatorial background. The K^0_S yield was determined in each bin using a fit function that describes both the signal and the background. A Lorentzian function was used for the signal:

$$L(m) = A\frac{1}{\pi}\frac{\frac{1}{2}\Gamma}{(m-m_0)^2 + (\frac{1}{2}\Gamma)^2}\,, \tag{3}$$

where A is the normalization factor, Γ is the full width at half maximum of the signal peak, and m_0 is the mass parameter. The background contribution is described by a polynomial function of 2^{nd} order. Figure 3 shows examples of $\pi^+\pi^-$ invariant mass distributions obtained from the $p_{beam} = 40$ GeV/c data set after all V^0 selection criteria for real data (*left*) and for simulated events (*right*).

The procedure of fitting the histograms proceeds in three steps. In the first step, the background outside of the signal peak ([0.475–0.525] GeV) is fitted with a polynomial of 2nd order. This step is necessary to obtain starting values for the parameters of the background function. In the next step, a full invariant mass spectrum fit is performed with the sum of the Lorentzian and the background function. The ini-

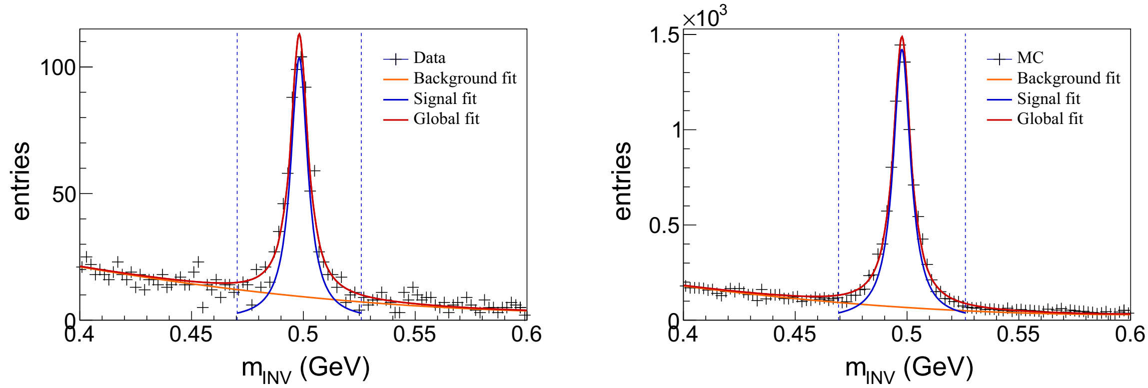

Fig. 3 The invariant mass distribution of K_S^0 candidates for experimental data (left) and MC (right) for the $p_{beam} = 40$ GeV/c data set for $-0.25 \leq y < 0.25$ and $0.2 \leq p_T < 0.4$ after all selection criteria. The dashed-blue vertical lines indicate the regions where the K_S^0 signal was integrated. The signal data points are black, the fitted background is orange, the fitted signal is blue, and the total fit results are red. Mass resolutions obtained from the fits are: $\sigma = (0.00925 \pm 0.00064)$ GeV for the experimental data and $\sigma = (0.00946 \pm 0.00017)$ GeV for the MC data

tial parameter values for the background function are taken from the previous step, the mass parameter is fixed to the PDG value of $m_0 = 0.497614(24)$ GeV [16], and the width is allowed to vary between 0.005 and 0.03 GeV. Finally, in the last step, all parameters are free, and the fitting region is [0.35−0.65] GeV. The orange and blue curves in Fig. 3 show the fitted polynomial background and the Lorentzian signal function. To minimize the sensitivity of the K_S^0 yield to the integration window, the uncorrected number of K_S^0 was calculated by subtracting bin-by-bin the fitted background (B) and summing the background-subtracted signal in the mass window $m_0 \pm 3\Gamma$ (dashed vertical lines), where m_0 is the fitted mass of the K_S^0. Figure 3 shows that the simulation reproduces the central value of the K_S^0 mass distribution and its width agree with the data within uncertainties. The Γ parameter fitted to the simulation was used to calculate the signal from the simulation. Thus, a possible bias due to differences between the data and the simulation is reduced; see Sect. 3.8.

The uncorrected bin-by-bin K_S^0 multiplicities and their statistical uncertainties are shown in Fig. 4.

3.6 Correction factors

A correction for interactions of the incident protons with the target vessel is not needed, because the distributions of the primary vertex coordinates show no sign of such events after the event and track selection criteria. A detailed Monte Carlo simulation was performed to compute the corrections for losses due to the trigger bias, geometrical acceptance, reconstruction efficiency, and the selection criteria applied in the analysis. The correction factors are based on 20×10^6 inelastic p+p events at each beam momenta $p_{beam} = 31, 40$ and 80 GeV/c produced by the EPOS1.99 event generator [19,20]. Particles in the generated events were tracked through the NA61/SHINE apparatus using the GEANT3 package [21]. The TPC response was simulated by dedicated software packages that account for known detector effects. The simulated events were reconstructed with the same software as the real events, and the same selection criteria were applied. However, dE/dx identification was replaced by matching reconstructed tracks to simulated ones. The branching ratio of K_S^0 decays is taken into account in the GEANT3 software package. For each y and p_T bin, the correction factor $c_{MC}(y, p_T)$ was calculated as:

$$c_{MC}(y, p_T) = \frac{n_{MC}^{gen}(y, p_T)}{N_{MC}^{gen}} \Bigg/ \frac{n_{MC}^{acc}(y, p_T)}{N_{MC}^{acc}} , \qquad (4)$$

where

- $n_{MC}^{gen}(y, p_T)$ is the number of K_S^0 generated in a given (y, p_T) bin,
- $n_{MC}^{acc}(y, p_T)$ is the number of reconstructed K_S^0 in a given (y, p_T) bin.
- N_{MC}^{gen} is the number of generated inelastic p+p interactions (20×10^6),
- N_{MC}^{acc} is the number of accepted p+p events (about 13.5×10^6 for all three beam momenta).

The loss of the K_S^0 mesons due to the dE/dx selection criteria is corrected with an additional factor:

$$c_{dE/dx} = \frac{1}{\epsilon^2} = 1.005 , \qquad (5)$$

where $\epsilon = 0.9973$ is the probability for the pions to be detected within $\pm 3\sigma$ around the nominal Bethe–Bloch value.

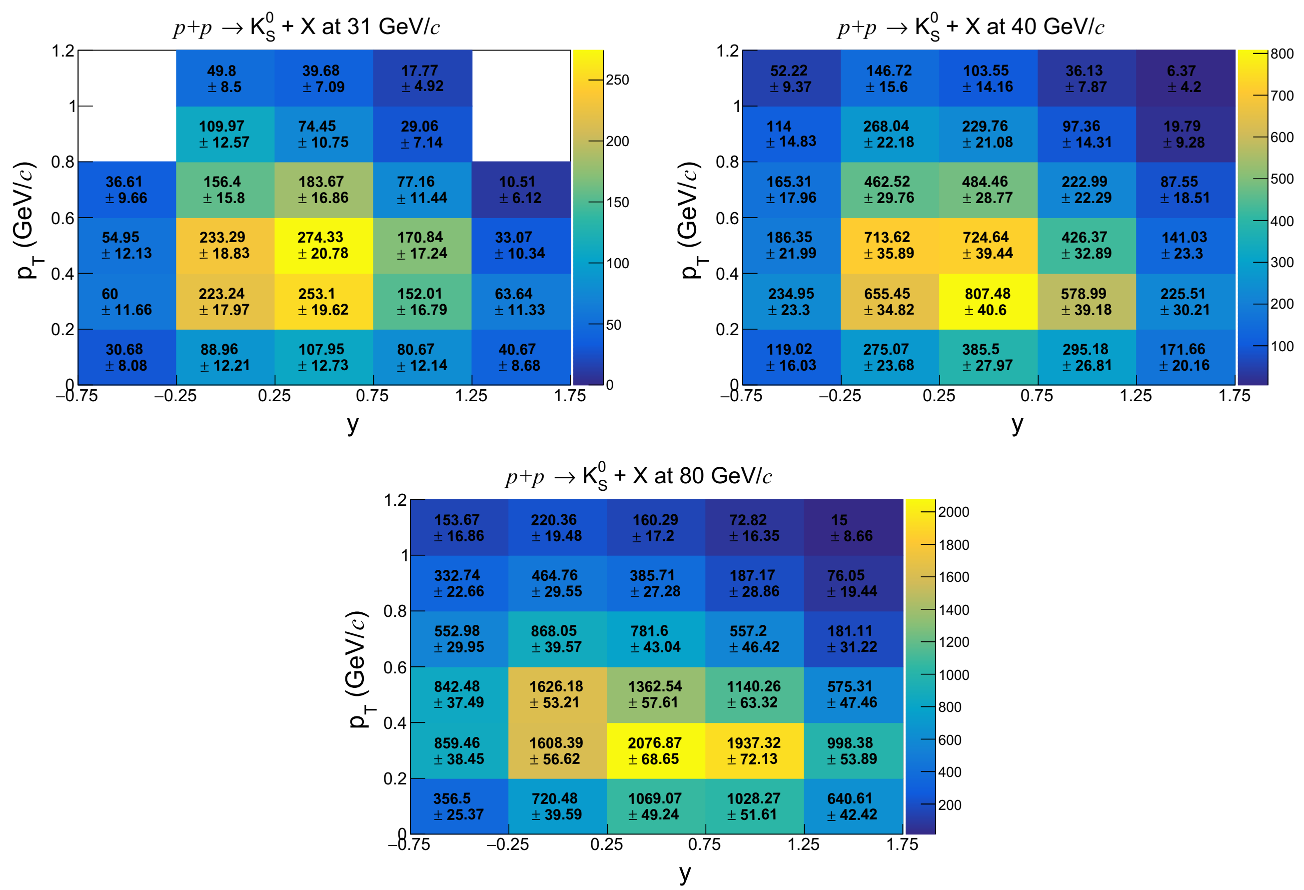

Fig. 4 Uncorrected bin-by-bin multiplicities of K^0_S with their statistical uncertainties for p_{beam} = 31 GeV/c (left), p_{beam} = 40 GeV/c (right) and p_{beam} = 80 GeV/c (bottom)

The double-differential yield of K^0_S per inelastic event in bins of (y, p_T) is calculated as follows:

$$\frac{d^2n}{dy\,dp_T}(y, p_T) = \frac{c_{dE/dx} \cdot c_{MC}(y, p_T)}{\Delta y\,\Delta p_T} \cdot \frac{n_{K^0_S}(y, p_T)}{N_{events}}, \quad (6)$$

where

– $c_{dE/dx}$, $c_{MC}(y, p_T)$ are the correction factors described above,
– Δy and Δp_T are the bin widths,
– $n_{K^0_S}(y, p_T)$ is the uncorrected number of K^0_S , obtained by the signal extraction procedure described in Sect. 3.5. The corresponding values are presented in Fig. 4,
– N_{events} is the number of events left in the sample after application of the selection criteria (Fig. 5).

3.7 Statistical uncertainties

The statistical uncertainties of the corrected double-differential yields (see Eq. 6) receive contributions from the statistical uncertainty of the correction factor $c_{MC}(y, p_T)$ and the statistical uncertainty of the uncorrected number of K^0_S ($\Delta N_{K^0_S}(y, p_T)$). The statistical uncertainty of the former receives two contributions: the first, α, caused by the loss of inelastic interactions due to the event selection and the second, β, connected with the loss of K^0_S candidates due to the V^0 selection:

$$c_{MC}(y, p_T) = \frac{n^{gen}_{MC}(y, p_T)}{N^{gen}_{MC}} \Bigg/ \frac{n^{acc}_{MC}(y, p_T)}{N^{acc}_{MC}} = \frac{N^{acc}_{MC}}{N^{gen}_{MC}} \Bigg/ \frac{n^{acc}_{MC}(y, p_T)}{n^{gen}_{MC}(y, p_T)} = \frac{\alpha}{\beta(y, p_T)}, \quad (7)$$

The error of α is calculated assuming a binomial distribution:

$$\Delta\alpha = \sqrt{\frac{\alpha(1-\alpha)}{N^{gen}_{MC}}}, \quad (8)$$

The error of β is calculated according to the formula:

$$\Delta\beta(y, p_T) = \sqrt{\left(\frac{\Delta n_{MC}^{acc}(y, p_T)}{n_{MC}^{gen}(y, p_T)}\right)^2 + \left(\frac{n_{MC}^{acc}(y, p_T) \cdot \Delta n_{MC}^{gen}(y, p_T)}{(n_{MC}^{gen}(y, p_T))^2}\right)^2}, \tag{9}$$

where $\Delta n_{MC}^{acc}(y, p_T) = \sqrt{S+B}$ see Sect. 3.5, and $\Delta n_{MC}^{gen}(y, p_T) = \sqrt{n_{MC}^{gen}(y, p_T)}$.

The equation for $\Delta c_{MC}(y, p_T)$ can be written as:

$$\Delta c_{MC}(y, p_T) = \sqrt{\left(\frac{\Delta\alpha}{\beta}\right)^2 + \left(-\frac{\alpha \cdot \Delta\beta}{\beta^2}\right)^2}. \tag{10}$$

Finally, the statistical uncertainties $\Delta n_{K_S^0}(y, p_T)$ of the corrected number of K_S^0 are:

$$\Delta \frac{d^2n}{dydp_T}(y, p_T) = \sqrt{\left(\frac{c_{dE/dx} \cdot c_{MC}(y, p_T)}{N_{events}\, \Delta y\, \Delta p_T}\right)^2 \Delta n_{K_S^0}^2(y, p_T) + \left(\frac{c_{dE/dx} \cdot n_{K_S^0}(y, p_T)}{N_{events}\, \Delta y\, \Delta p_T}\right)^2 \Delta c_{MC}^2(y, p_T)}. \tag{11}$$

3.8 Systematic uncertainties

Three possible groups of contributions to the systematic uncertainties related to the event selection criteria, the track and V^0 selection criteria and the signal extraction procedure were considered.

(i) The uncertainties related to the event selection criteria (see Sect. 3.3) were estimated by performing the analysis with the following changes:

- Simulations were done with and without the S4 trigger condition for all inelastic *p+p* interactions. One-half of the difference between these two results was taken as the contribution to the systematic uncertainty, which amounts to up to 3%.
- The allowed range of the vertex z position was changed from -590 $<$ z (cm) < -572 to $-588 <$ z (cm) < -574 and $-592 <$ z (cm) < -570. The uncertainty due to the variation of the selection window amounts to up to 4%.

(ii) The uncertainties related to the track and V^0 selection criteria were estimated by performing the analysis with the following changes compared to the original values (see Sect. 3.4):

- the minimum required number of clusters in both VTPCs for V^0 daughters was changed from 15 to 12 and 18, indicating a possible bias of up to 2%,
- the standard d$E/$dx selection criteria used for identification of V^0 daughters was changed from $\pm 3\sigma$ to $\pm 2.5\sigma$ and $\pm 3.5\sigma$ from the nominal Bethe-Bloch value indicating a possible bias of up to 3%,
- the Δz selection criteria was changed by varying the parameters a and b from 1.91 to 2.01 and 1.81 for parameter a and from 0.99 to 0.98 and 1.00 for parameter b for $p_{beam} = 31$ GeV/c, from 1.71 to 1.91 and 1.51 for parameter a and from 0.95 to 0.93 and 0.97 for parameter b for $p_{beam} = 40$ GeV/c and from 1.85 to 2.05 and 1.65 for parameter a and from 0.90 to 0.88 and 0.92 for parameter b for $p_{beam} = 80$ GeV/c, indicating a possible bias of up to 2%,
- the allowed distance of closest approach of the K_S^0 trajectory to the primary vertex was varied from 0.25 to 0.20 and 0.30 cm, indicating a possible bias of up to 3%,
- the $cos\Theta^*$ range for accepted candidates was changed from $-0.97 < cos\Theta^* < 0.85$ to $-0.99 < cos\Theta^* < 0.87$ and $-0.95 < cos\Theta^* < 0.83$ indicating a possible bias of up to 3%.

(iii) The uncertainty due to the signal extraction procedure (see Sect. 3.5) was estimated by:

- changing the background fit function from a 2^{nd} order to a 3^{rd} order polynomial indicating a possible bias of up to 4%,
- changing the invariant mass range over which the uncorrected number of K_S^0 was integrated from $m_0 \pm 3\Gamma$ to $m_0 \pm 2.5\Gamma$ and $m_0 \pm 3.5\Gamma$ indicating a possible bias of up to 2%,
- calculating the uncorrected number of K_S^0 as the sum of entries after background fit subtraction instead of

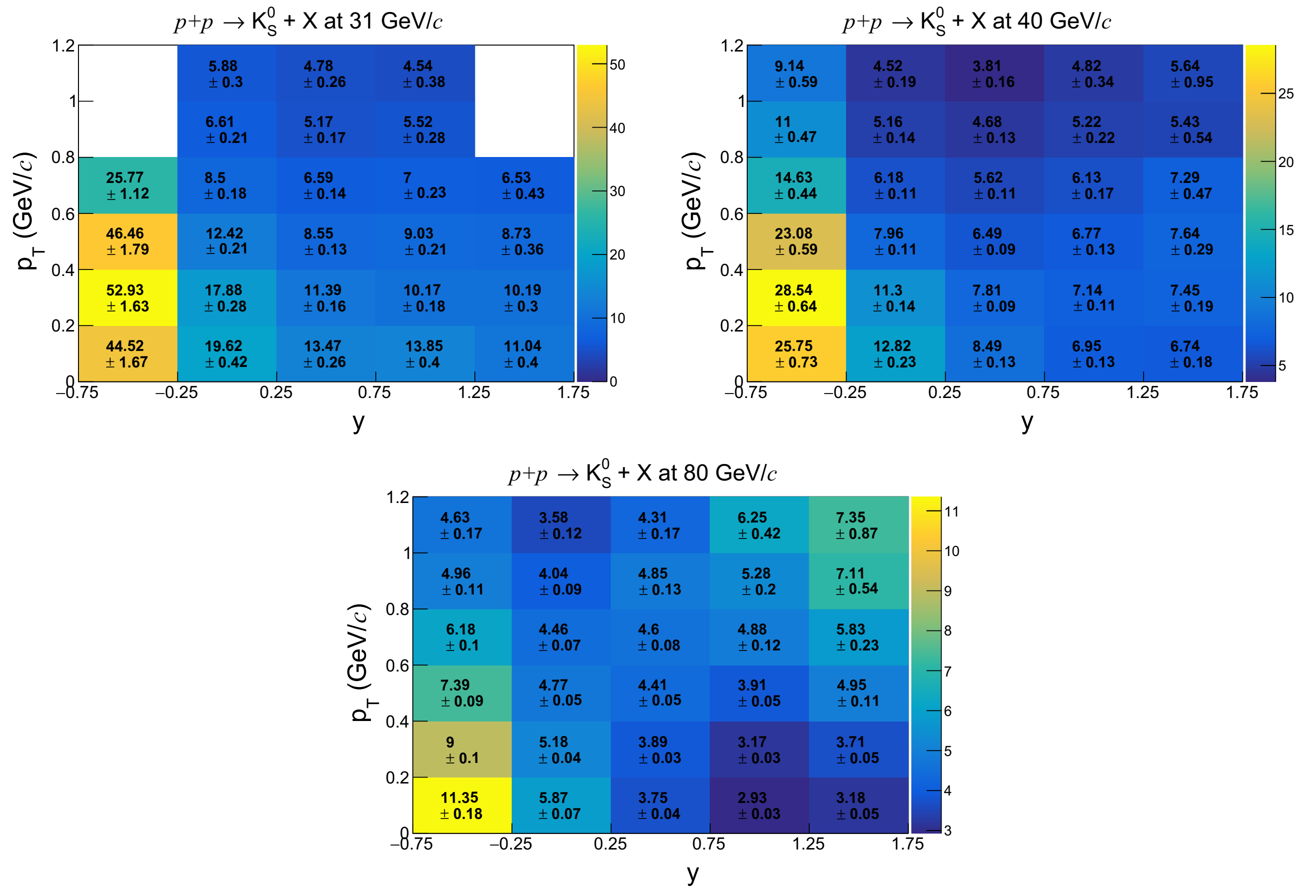

Fig. 5 Monte-Carlo correction factors (see Eq. 4) with their statistical uncertainties (see Eq. 10) in each (y, p_T) bin for $p_{beam} = 31$ GeV/c (left), $p_{beam} = 40$ GeV/c (right) and $p_{beam} = 80$ GeV/c (bottom)

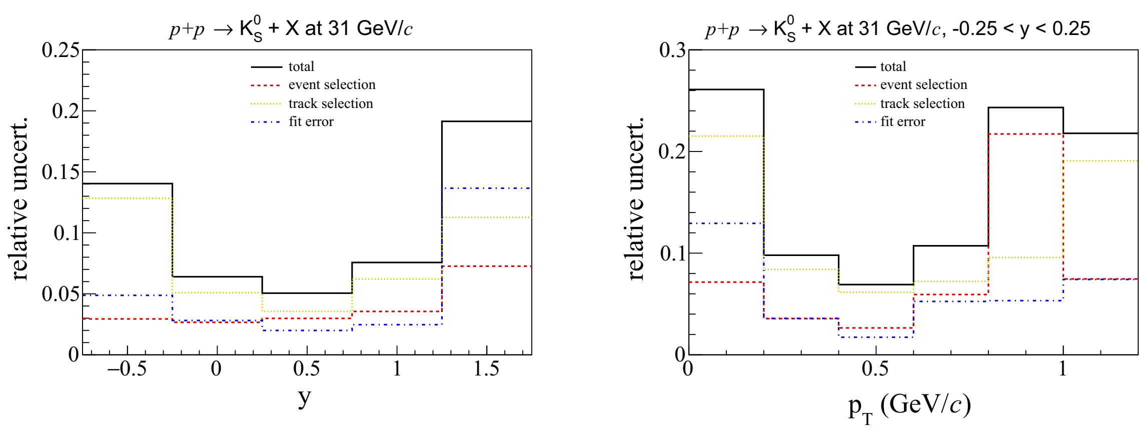

Fig. 6 Systematic uncertainties relative to the measured yield of double-differential distributions integrated in p_T shown in dependence on rapidity y at $p_{beam} = 31$ GeV/c ($left$). Systematic uncertainties relative to the measured yield of double-differential distributions in y and p_T shown in dependence on transverse momentum p_T at mid-rapidity at $p_{beam} = 31$ GeV/c ($right$)

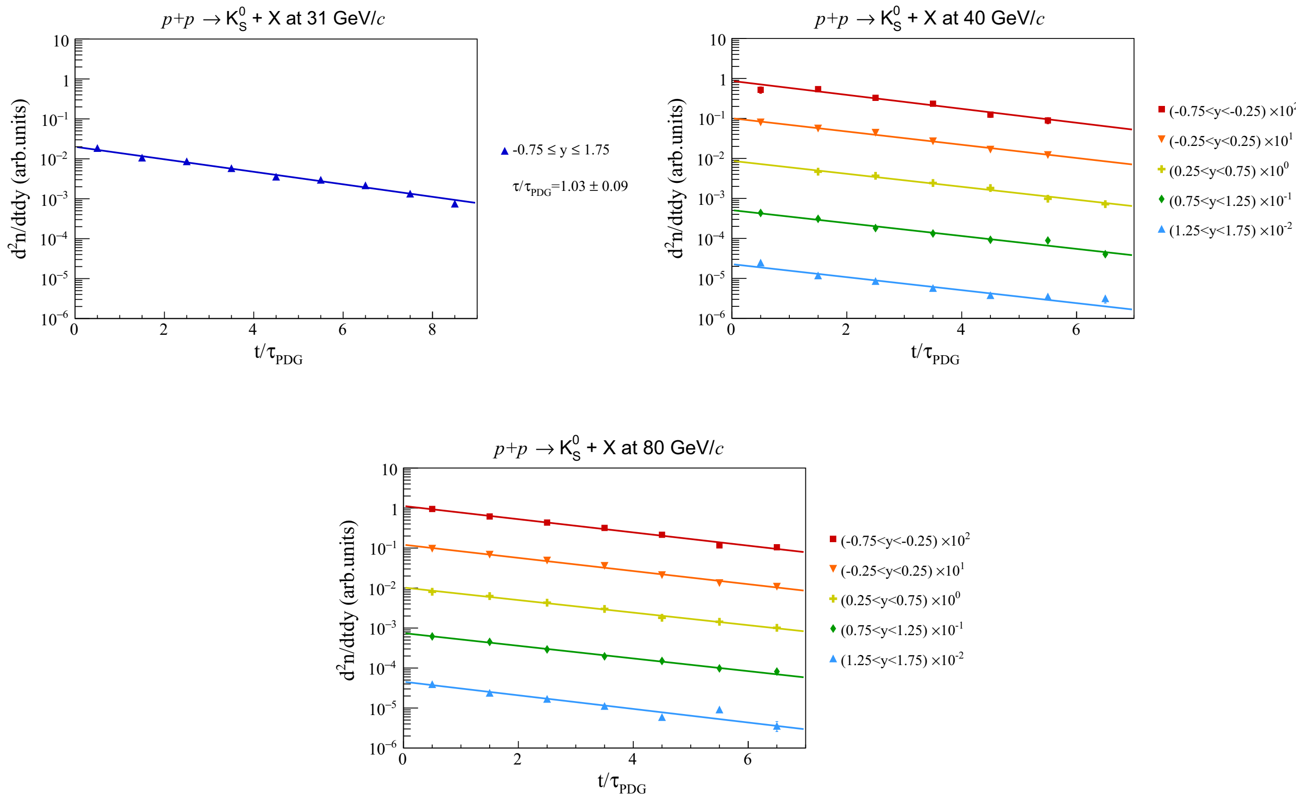

Fig. 7 Corrected lifetime distributions for K^0_S mesons produced in inelastic p+p interactions at beam energies of p_{beam} = 31 GeV/c (top left), p_{beam} = 40 GeV/c (top right), and p_{beam} = 80 GeV/c (bottom). The straight lines show the results of exponential fits used to obtain the mean lifetimes (normalized to the PDG value) in rapidity bins. Statistical uncertainties are smaller than the marker size and are not visible on the plots

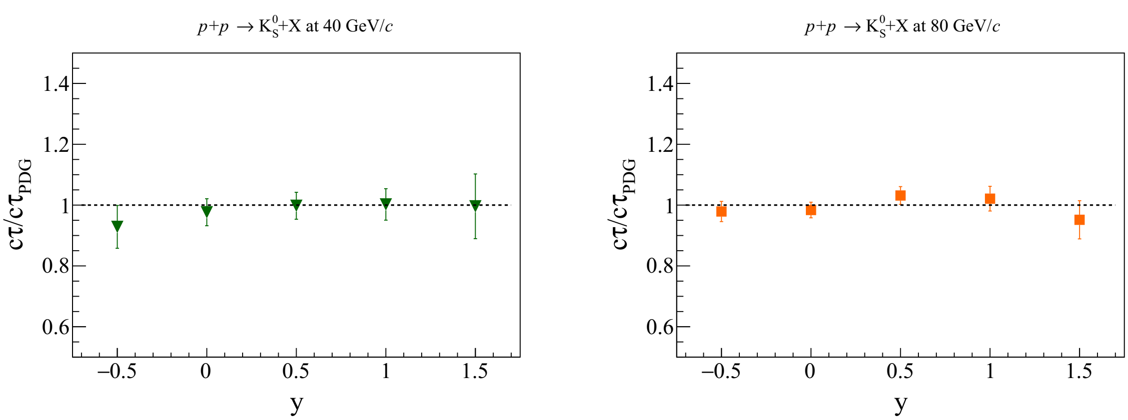

Fig. 8 Mean K^0_S lifetimes (normalized to the PDG value) obtained from fits to the lifetime distributions of Fig. 7 for the p_{beam} = 40 GeV/c (left) and p_{beam} = 80 GeV/c (right) data sets versus the rapidity y. The error bars indicate the statistical uncertainties

the integral of the Lorentzian signal function indicating a possible bias of up to 2%,
- changing the region of the fit from [0.35−0.65] GeV/c^2 to [0.38−0.62] GeV/c^2 indicating a possible bias of up to 2%.

The maximum deviations are determined for every group of possible sources, which contribute to the systematic uncertainty. The systematic uncertainty was calculated as the square root of the sum of squares of the described possible biases assuming that they are uncorrelated. This procedure was used to estimate systematic uncertainties of all final quantities presented in this paper: yields in (y, p_T) bins,

Table 2 Double differential K_S^0 yields in bins of (y, p_T). The first uncertainty is statistical, while the second one is systematic

Momentum		Results $\frac{d^2n}{dydp_T} \times 10^3$		
	y	p_T (GeV/c)		
$p_{beam} = 31$ GeV/c		(0.0; 0.2)	(0.2; 0.4)	(0.4; 0.6)
	(−0.75; −0.25)	19.2 ± 5.1 ± 11.4	44.6 ± 8.8 ± 8.4	35.9 ± 8.0 ± 15.3
	(−0.25; 0.25)	24.5 ± 3.4 ± 6.4	56.1 ± 4.6 ± 5.5	40.7 ± 3.4 ± 2.9
	(0.25; 0.75)	20.4 ± 2.5 ± 2.6	40.5 ± 3.2 ± 2.6	33.0 ± 2.6 ± 3.0
	(0.75; 1.25)	15.7 ± 2.4 ± 6.8	21.7 ± 2.5 ± 2.7	21.7 ± 2.3 ± 2.5
	(1.25; 1.75)	6.3 ± 1.4 ± 2.7	9.1 ± 1.7 ± 1.8	4.1 ± 1.3 ± 1.4
	y	p_T (GeV/c)		
		(0.6; 0.8)	(0.8; 1.0)	(1.0; 1.2)
	(−0.75; −0.25)	13.3 ± 3.6 ± 4.2	–	–
	(−0.25; 0.25)	18.7 ± 2.0 ± 2.0	10.2 ± 1.2 ± 2.5	4.2 ± 0.8 ± 0.9
	(0.25; 0.75)	17.0 ± 1.6 ± 1.8	5.4 ± 0.8 ± 0.7	2.7 ± 0.5 ± 0.5
	(0.75; 1.25)	7.6 ± 1.2 ± 0.6	2.3 ± 0.6 ± 0.9	1.2 ± 0.4 ± 0.3
	(1.25; 1.75)	1.0 ± 0.6 ± 0.5	–	–
	y	p_T (GeV/c)		
$p_{beam} = 40$ GeV/c		(0.0; 0.2)	(0.2; 0.4)	(0.4; 0.6)
	(−0.75; −0.25)	24.8 ± 3.5 ± 10.5	54.3 ± 5.6 ± 9.7	34.9 ± 4.3 ± 5.2
	(−0.25; 0.25)	28.6 ± 2.6 ± 1.9	60.0 ± 3.3 ± 4.4	46.0 ± 2.4 ± 1.7
	(0.25; 0.75)	26.5 ± 2.0 ± 3.8	51.1 ± 2.7 ± 3.8	38.1 ± 2.2 ± 4.2
	(0.75; 1.25)	16.6 ± 1.6 ± 1.0	33.5 ± 2.4 ± 4.1	23.4 ± 1.9 ± 2.3
	(1.25; 1.75)	9.4 ± 1.2 ± 1.6	13.6 ± 1.9 ± 3.8	8.7 ± 1.5 ± 1.5
	y	p_T (GeV/c)		
		(0.6; 0.8)	(0.8; 1.0)	(1.0; 1.2)
	(−0.75; −0.25)	19.6 ± 2.3 ± 2.4	10.2 ± 1.4 ± 2.4	3.9 ± 0.8 ± 1.1
	(−0.25; 0.25)	23.2 ± 1.6 ± 2.2	11.2 ± 1.0 ± 1.3	5.4 ± 0.7 ± 0.7
	(0.25; 0.75)	22.1 ± 1.4 ± 2.5	8.7 ± 0.9 ± 1.8	3.2 ± 0.5 ± 0.6
	(0.75; 1.25)	11.1 ± 1.2 ± 1.2	4.1 ± 0.7 ± 0.6	1.4 ± 0.4 ± 0.3
	(1.25; 1.75)	5.2 ± 1.2 ± 2.8	0.9 ± 0.5 ± 0.3	0.3 ± 0.2 ± 0.1
	y	p_T (GeV/c)		
$p_{beam} = 80$ GeV/c		(0.0; 0.2)	(0.2; 0.4)	(0.4; 0.6)
	(−0.75; −0.25)	35.2 ± 2.5 ± 5.0	64.2 ± 2.9 ± 3.6	51.8 ± 2.4 ± 3.2
	(−0.25; 0.25)	35.0 ± 2.0 ± 3.0	68.6 ± 2.5 ± 2.5	63.8 ± 2.2 ± 2.7
	(0.25; 0.75)	33.0 ± 1.6 ± 1.2	67.6 ± 2.3 ± 2.7	49.7 ± 2.2 ± 3.5
	(0.75; 1.25)	23.6 ± 1.3 ± 1.3	50.8 ± 2.0 ± 2.4	35.3 ± 2.1 ± 2.3
	(1.25; 1.75)	15.5 ± 1.2 ± 0.9	30.8 ± 1.7 ± 1.9	20.5 ± 1.9 ± 2.0
	y	p_T (GeV/c)		
		(0.6; 0.8)	(0.8; 1.0)	(1.0; 1.2)
	(−0.75; −0.25)	28.0 ± 1.6 ± 2.0	13.4 ± 1.0 ± 0.8	5.6 ± 0.7 ± 0.6
	(−0.25; 0.25)	31.6 ± 1.5 ± 2.0	15.4 ± 1.0 ± 1.3	6.4 ± 0.6 ± 0.6
	(0.25; 0.75)	29.3 ± 1.7 ± 2.2	14.7 ± 1.2 ± 1.5	5.4 ± 0.7 ± 0.5
	(0.75; 1.25)	22.0 ± 2.0 ± 1.8	7.4 ± 1.3 ± 1.3	3.4 ± 0.9 ± 0.3
	(1.25; 1.75)	8.5 ± 1.6 ± 2.1	4.6 ± 1.2 ± 1.8	0.8 ± 0.6 ± 0.3

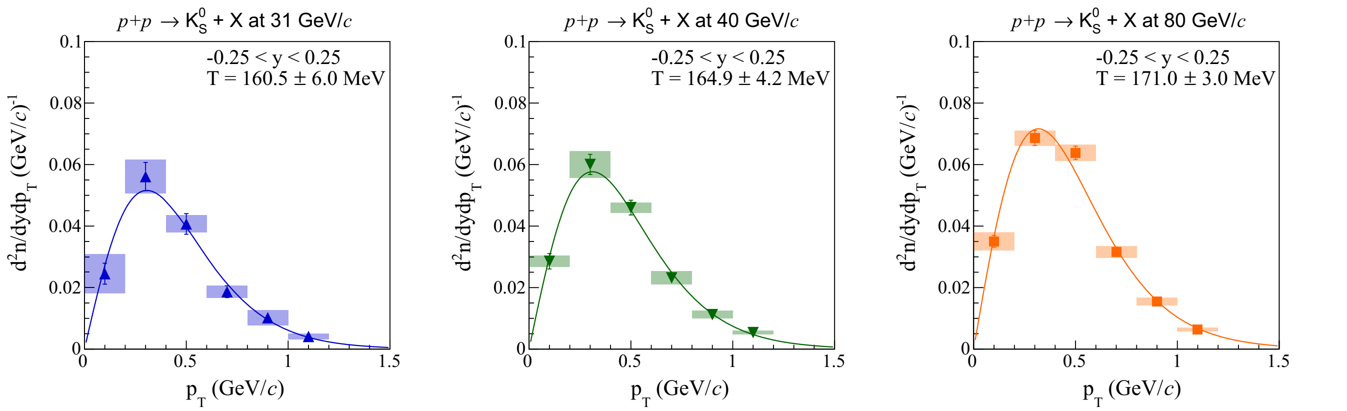

Fig. 9 Double-differential K^0_S spectra in inelastic p+p interactions at 31 GeV/c (left), 40 GeV/c (middle) and 80 GeV/c (right) at mid-rapidity ($y \approx 0$) calculated according to Eq. 6. Measured points are shown as blue full triangles up (for $p_{beam} = 31$ GeV/c), green full triangles down (for $p_{beam} = 40$ GeV/c) and orange full squares (for $p_{beam} = 80$ GeV/c). The solid curves are fitted to the data points using the exponential function (Eq. 12). Vertical bars indicate statistical uncertainties (for some points smaller than the symbol size). Shaded boxes show systematic uncertainties. Only statistical uncertainties are taken into account in the fit, because the systematic uncertainties do not depend on p_T. The numerical values of the data points are listed in Table 2

Table 3 Numerical values of T and dn/dy for K^0_S mesons produced in p+p interactions at 31, 40 and 80 GeV/c. The first column indicates the data set. The second column shows the rapidity range. The values of the inverse slope parameter are listed in the third column, along with their statistical and systematic uncertainties. The last column shows the numerical values of the p_T-integrated yields presented in Fig. 10 with statistical and systematic uncertainties

$p_{beam} = 31$ GeV/c	y	T (MeV)	$\frac{dn}{dy} \times 10^3$
	$(-0.75; -0.25)$	$149.4 \pm 18.7 \pm 30.9$	$24.6 \pm 2.8 \pm 3.5$
	$(-0.25; 0.25)$	$160.5 \pm 5.9 \pm 7.4$	$31.3 \pm 1.5 \pm 2.0$
	$(0.25; 0.75)$	$152.5 \pm 4.9 \pm 4.4$	$24.1 \pm 1.1 \pm 1.2$
	$(0.75; 1.25)$	$137.0 \pm 6.2 \pm 11.8$	$14.1 \pm 0.9 \pm 1.1$
	$(1.25; 1.75)$	$93.5 \pm 11.7 \pm 15.1$	$4.2 \pm 0.6 \pm 0.8$
$p_{beam} = 40$ GeV/c	y	T (MeV)	$\frac{dn}{dy} \times 10^3$
	$(-0.75; -0.25)$	$162.6 \pm 6.8 \pm 12.8$	$30.0 \pm 1.7 \pm 3.5$
	$(-0.25; 0.25)$	$164.8 \pm 4.2 \pm 2.2$	$35.5 \pm 1.0 \pm 1.9$
	$(0.25; 0.75)$	$157.4 \pm 3.7 \pm 4.6$	$30.4 \pm 0.9 \pm 3.1$
	$(0.75; 1.25)$	$143.6 \pm 4.5 \pm 3.3$	$18.2 \pm 0.8 \pm 1.4$
	$(1.25; 1.75)$	$122.2 \pm 7.6 \pm 6.3$	$7.6 \pm 0.6 \pm 0.7$
$p_{beam} = 80$ GeV/c	y	T (MeV)	$\frac{dn}{dy} \times 10^3$
	$(-0.75; -0.25)$	$165.8 \pm 3.6 \pm 3.3$	$40.3 \pm 1.0 \pm 1.9$
	$(-0.25; 0.25)$	$171.0 \pm 3.0 \pm 2.3$	$45.1 \pm 0.9 \pm 1.7$
	$(0.25; 0.75)$	$168.0 \pm 3.4 \pm 3.0$	$40.7 \pm 0.8 \pm 1.4$
	$(0.75; 1.25)$	$159.9 \pm 4.7 \pm 5.8$	$28.9 \pm 0.8 \pm 1.0$
	$(1.25; 1.75)$	$140.6 \pm 6.2 \pm 4.5$	$16.2 \pm 0.7 \pm 0.9$

inverse slope parameters of transverse momentum spectra, yields in rapidity bins, and mean multiplicities. Examples of the relative contributions of each of the listed sources to the systematic uncertainties of the final spectra are shown in Fig. 6 for the $p_{beam} = 31$ GeV/c data set. The uncertainties are similar for the other two data sets.

3.9 Mean lifetime measurements

The reliability of the K^0_S reconstruction and the correction procedure was validated by studying the lifetime distribution of the analyzed K^0_S. The lifetime ($c\tau$) of each identified K^0_S was calculated from the V^0 path length and its velocity. The corrected number of K^0_S was then determined in bins of $c\tau/c\tau_{PDG}$, and for the five rapidity bins of the $p_{beam} = 40$ GeV/c and 80 GeV/c data sets and in the whole rapidity range ($-0.75 < y < 1.75$) of the $p_{beam} = 31$ GeV/c data set (see Fig. 7). The straight lines in Fig. 7 represent the results of exponential fits, which provide mean lifetime values (normalized to the known PDG value [16]) as a function of rapidity. The thus determined mean lifetimes are shown in Fig. 8 as a function of rapidity. The measured mean K^0_S lifetimes agree within uncertainties with the PDG value and thus confirm the quality of the analysis.

4 Results

This section presents new NA61/SHINE results on inclusive K^0_S meson production from inelastic $p+p$ interactions at beam momenta of 31, 40 and 80 GeV/c. Transverse momentum and rapidity spectra are obtained from the analysis of the weak decays of K^0_S mesons into two charged pions.

4.1 Transverse momentum spectra

Double differential K^0_S yields listed in Table 2 represent the main result of this paper.

Yields are determined in five consecutive rapidity bins in the interval $-0.75 < y < 1.75$ and six transverse momentum bins in the interval $0.0 < p_T$ (GeV/c) < 1.2. The transverse momentum distributions at mid-rapidity ($y \approx 0$) are shown in Fig. 9.

An exponential function was fitted to the transverse momentum spectra. It reads:

$$f(p_T) = A \cdot p_T \cdot \exp\left(\frac{\sqrt{p_T^2 + m_0^2}}{T}\right), \quad (12)$$

where m_0 is the mass of the K^0_S and T is the inverse slope parameter. The resulting values of T in each rapidity bin are listed in Table 3.

4.2 Rapidity distributions and mean multiplicities

Kaon yields in each rapidity bin were obtained from the measured transverse momentum distributions. The small fraction of K^0_S at high p_T outside of the acceptance was determined using Eq. 12. The resulting $\frac{dn}{dy}$ spectra of K^0_S mesons produced in inelastic $p+p$ interactions at 31, 40 and 80 GeV/c are presented in Fig. 10 together with the previous NA61/SHINE results obtained for $p+p$ interactions at 158 GeV/c [5].

The mean multiplicities of K^0_S mesons were calculated as the sum of the measured data points in Fig. 10 scaled by the ratio between measured and unmeasured regions obtained from the Monte-Carlo simulation. The unmeasured region was minimized by using the yields at positive rapidity as input for the yields at negative rapidity when necessary. The fraction of the unmeasured regions relative to the total yields are 2.2% for $p_{beam} = 31$ GeV/c, 3.1% for $p_{beam} = 40$ GeV/c and 6.5% for $p_{beam} = 80$ GeV/c. The statistical uncertainties of $\langle K^0_S \rangle$ were calculated as the square root of the sum of the squares of the statistical uncertainties of the contributing bins. The systematic uncertainties were calculated as the square root of squares of systematic uncertainties described in Sect. 3.8 and half of the extrapolated yield. The mean multiplicities of K^0_S mesons in inelastic $p+p$ collisions were found to be $0.0595 \pm 0.0019(stat) \pm 0.0030(sys)$ at 31 GeV/c, $0.0761 \pm 0.0013(stat) \pm 0.0043(sys)$ at 40 GeV/c and $0.1158 \pm 0.0012(stat) \pm 0.0055(sys)$ at 80 GeV/c.

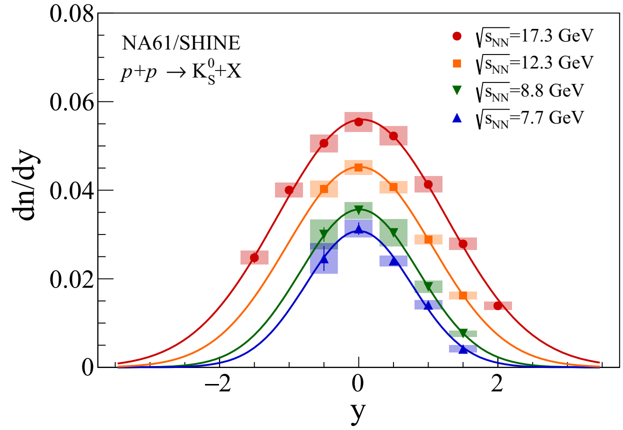

Fig. 10 Rapidity distribution dn/dy obtained by p_T-integration of data and extrapolation. Statistical uncertainties are shown by vertical bars (often smaller than the marker size), while shaded boxes indicate systematic uncertainties. The curves indicate the result of the Gaussian fit to the measured points. Points for $p+p$ at $\sqrt{s_{NN}} = 17.3$ GeV are taken from [5]

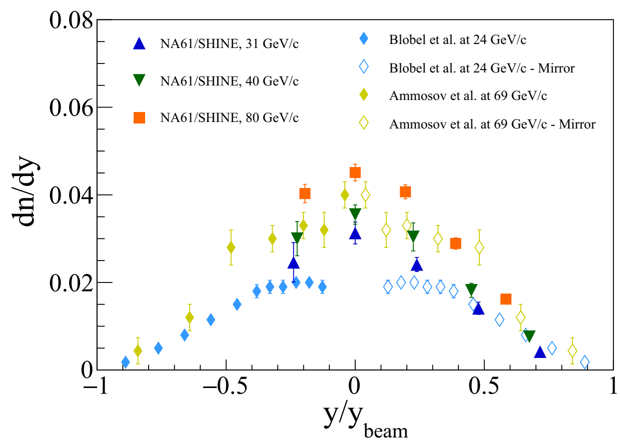

Fig. 11 dn/dy as a function of scaled rapidity y/y_{beam} of K^0_S mesons in inelastic $p+p$ interactions at 31, 40 and 80 GeV/c. Measured points are shown as blue full triangles up (for $p_{beam} = 31$ GeV/c), green full triangles down (for $p_{beam} = 40$ GeV/c) and orange full squares (for $p_{beam} = 80$ GeV/c). Results from other experiments are shown as azure-colored diamonds (for Blobel et al. at 24 GeV/c) and yellow-colored diamonds (for Ammosov et al. at 69 GeV/c). Vertical bars indicate total uncertainties (for some points smaller than the symbol size)

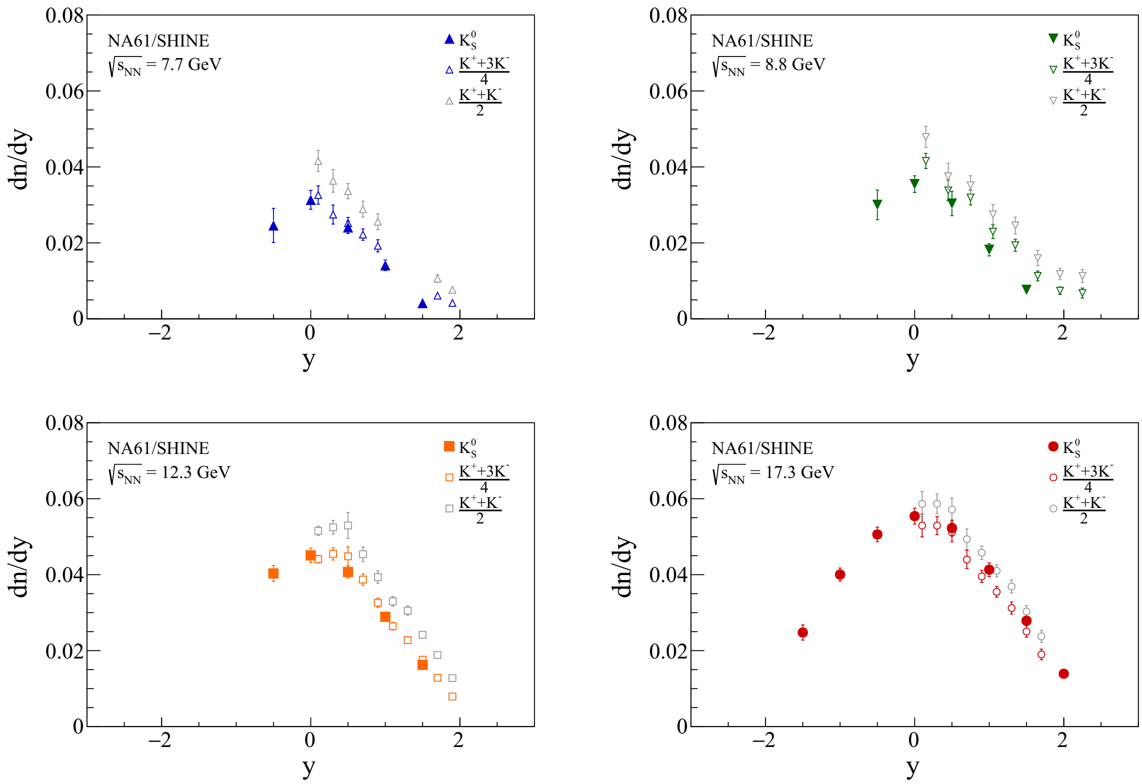

Fig. 12 Rapidity distribution dn/dy of K^0_S mesons in inelastic p+p interactions at 31, 40, 80 and 158 GeV/c. Measured points are shown as blue full triangles up for p_{beam} = 31 GeV/c (top left), green full triangles down for p_{beam} = 40 GeV/c (top right), orange full squares for p_{beam} = 80 GeV/c (bottom left) and red full circles for p_{beam} = 158 GeV/c (bottom right). Results for charged kaons obtained by formula $\frac{1}{4}(N_{K^+} + 3 \cdot N_{K^-})$ are shown by open colored symbols for all data sets, while the results obtained by formula $\frac{1}{2}(N_{K^+} + N_{K^-})$ are shown by grey opened symbols. Vertical bars indicate total uncertainties (for some points smaller than the symbol size)

5 Comparison with published world data and model calculations

This section compares the new NA61/SHINE measurements of K^0_S production in inelastic p+p interactions at 31, 40 and 80 GeV/c with world data as well as with microscopic model calculations (Epos1.99 [19,20], SMASH 2.0 [22] and PHSD [23,24]). The K^0_S rapidity spectra from NA61/SHINE are compared in Fig. 11 to the results from Blobel et al. [25] as well as with results from Ammosov et al. [26]. The results from Blobel et al. at 24 GeV/c are significantly below the NA61/SHINE 31 GeV/c data in the central rapidity part. The results from Ammosov et al. at 69 GeV/c are located between the measured NA61/SHINE points of the 40 and 80 GeV/c data sets, as expected.

Recently NA61/SHINE reported an excess of charged over neutral kaon production in Ar+Sc collisions at 75A GeV/c [27]. The precise and detailed results on K^0_S production in p+p interactions reported here, together with the corresponding results on charged kaons [6], may contribute to the understanding of this puzzle. To this end the rapidity distributions of K^0_S are compared with two predictions derived from K^+ and K^- yields obtained from the same data sets [6]. The first prediction is based on valence- and sea-quark counting arguments [28] and leads to the equation $N_{K^0_S} = \frac{1}{4}(N_{K^+} + 3 \cdot N_{K^-})$. This relation was used in the past to estimate the neutral kaon flux in the fragmentation region for K^0 beam studies [29]. The second prediction assumes isospin symmetry of the different charge states of the kaon: $N_{K^0_S} = \frac{1}{2}(N_{K^+} + N_{K^-})$. The K^0_S rapidity distributions are compared to these two predictions in Fig. 12. The prediction based on valence quark counting describes the K^0_S rapidity distributions significantly better than the one assuming isospin symmetry.

Figure 13 compares the NA61/SHINE measurements with model calculations from Epos1.99, PHSD and SMASH 2.0. Epos1.99 overpredicts the experimental data at all three data beam momenta. PHSD overpredicts the measured p_{beam} = 80 GeV/c data, while for the remaining two data sets it shows fair agreement. SMASH 2.0 describes the experimental p_{beam} = 80 GeV/c data very well but underpredicts the remaining two data sets. All models exhibit the same shape of the rapidity distribution as the experimental data.

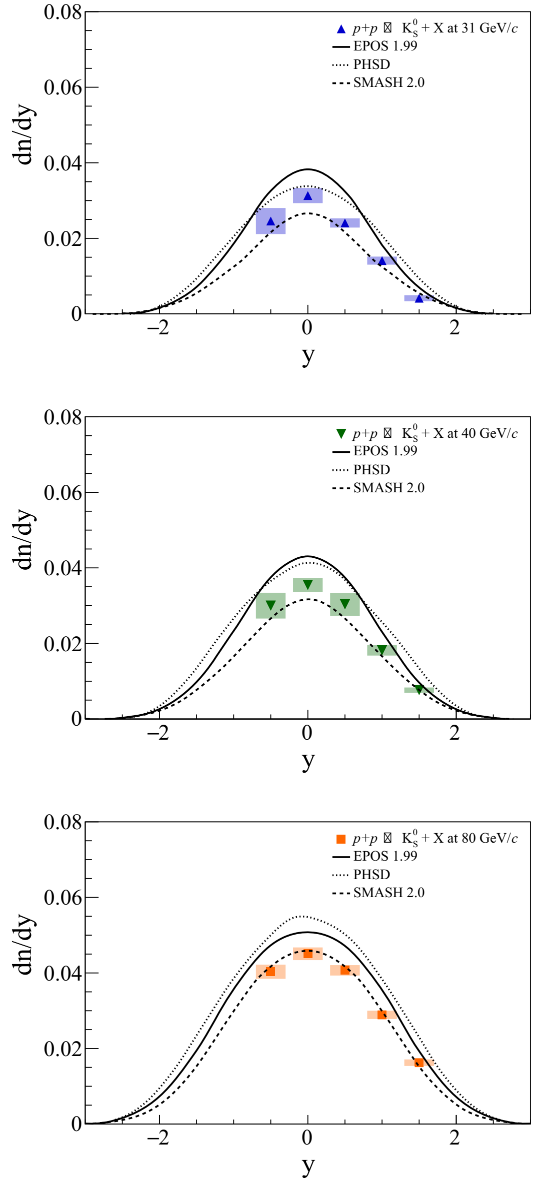

Fig. 13 Comparison of the experimental K^0_S rapidity distributions with model calculations. Colored symbols show the new measurements of NA61/SHINE as follows: p_{beam} = 31 GeV/c (top), p_{beam} = 40 GeV/c (middle) and p_{beam} = 80 GeV/c (bottom). The black curves show the result of the model calculations: EPOS1.99 (solid), PHSD (dotted) and SMASH 2.0 (dashed)

The mean multiplicity of K^0_S mesons in $p+p$ collisions at $\sqrt{s_{NN}}$ = 7.7, 8.8, 12.3 GeV, reported here, and the published result at $\sqrt{s_{NN}}$ = 17.3 GeV [5] are compared in Fig. 14 with the world data in the range from 3 - 32 GeV. The measured values are seen to rise linearly with collision energy $\sqrt{s_{NN}}$.

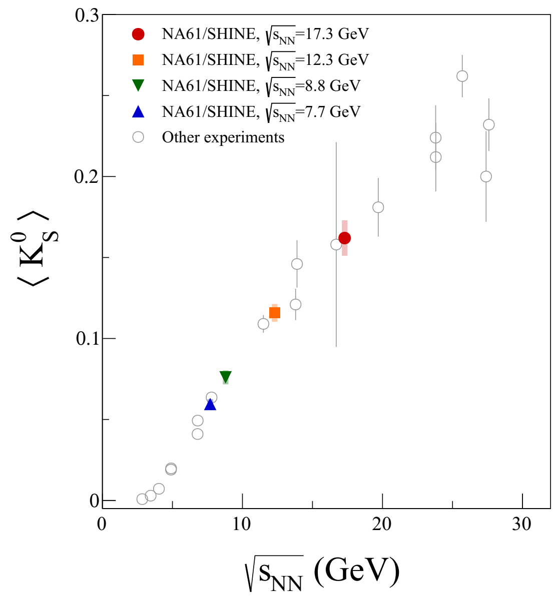

Fig. 14 Collision energy dependence of mean multiplicity of K^0_S mesons produced in $p+p$ interactions. The measurements from NA61/SHINE are shown with colored symbols as follows: blue full triangle up for p_{beam} = 31 GeV/c, green full triangle down for p_{beam} = 40 GeV/c, orange full square for p_{beam} = 80 GeV/c and red full circle for p_{beam} = 158 GeV/c [5]. The results published by other experiments are shown by the grey open circles [25,26,30–43]. Statistical uncertainties are smaller than the marker size, while shaded boxes indicate systematic uncertainties

6 Summary

This paper presents the new NA61/SHINE measurement of K^0_S mesons via their $\pi^+\pi^-$ decay mode in inelastic $p+p$ collisions at beam momenta of 31, 40 and 80 GeV/c ($\sqrt{s_{NN}}$ = 7.7, 8.8 and 17.3 GeV). Spectra of transverse momentum (up to 1.2 GeV/c), as well as a distributions of rapidity (from −0.75 to 1.75), are presented. The mean multiplicities, obtained from p_T-integrated spectra and extrapolated rapidity distributions, are $(5.95 \pm 0.19 \pm 0.30) \times 10^{-2}$ at 31 GeV/c, $(7.61 \pm 0.13 \pm 0.43) \times 10^{-2}$ at 40 GeV/c and $(11.58 \pm 0.12 \pm 0.55) \times 10^{-2}$ at 80 GeV/c, where the first uncertainty is statistical and the second systematic. The measured K^0_S lifetime agrees within small uncertainties with the PDG value and thus confirms the quality of the analysis. The mean multiplicities from model calculations deviate by up to 20% from the measurements. The SMASH 2.0 model provides the best description for p_{beam} = 31 and 80 GeV/c, while the PHSD model has the best agreement with measured data for p_{beam} = 40 GeV/c. The results of K^0_S production in proton–proton interactions presented in this paper significantly improve, with their high statistical and systematic precision, the knowledge of strangeness production in elementary interactions and will serve as a reference for studies of strange hadron production in nucleus–nucleus collisions.

Acknowledgements We would like to thank the CERN EP, BE, HSE and EN Departments for the strong support of NA61/SHINE.

Funding This work was supported by the Hungarian Scientific Research Fund (grant NKFIH 138136/137812/138152 and TKP2021-NKTA-64), the Polish Ministry of Science and Higher Education (DIR/WK/2016/ 2017/10-1, WUT ID-UB), the National Science Centre Poland (grants 2014/ 14/ E/ ST2/ 00018, 2016/ 21/ D/ ST2/ 01983, 2017/ 25/ N/ ST2/ 02575, 2018/ 29/ N/ ST2/ 02595, 2018/ 30/ A/ ST2/ 00226, 2018/ 31/ G/ ST2/ 03910, 2020/ 39/ O/ ST2/ 00277), the Norwegian Financial Mechanism 2014–2021 (grant 2019/ 34/ H/ ST2/ 00585), the Polish Minister of Education and Science (contract No. 2021/ WK/ 10), the European Union's Horizon 2020 research and innovation programme under grant agreement No. 871072, the Ministry of Education, Culture, Sports, Science and Technology, Japan, Grant-in-Aid for Scientific Research (grants 18071005, 19034011, 19740162, 20740160 and 20039012,22H04943), the German Research Foundation DFG (grants GA 1480/8-1 and project 426579465), the Bulgarian Ministry of Education and Science within the National Roadmap for Research Infrastructures 2020–2027, contract No. D01-374/18.12.2020, Serbian Ministry of Science, Technological Development and Innovation (grant OI171002), Swiss Nationalfonds Foundation (grant 200020117913/1), ETH Research Grant TH-01 07-3, National Science Foundation grant PHY-2013228 and the Fermi National Accelerator Laboratory (Fermilab), a U.S. Department of Energy, Office of Science, HEP User Facility managed by Fermi Research Alliance, LLC (FRA), acting under Contract No. DE-AC02-07CH11359 and the IN2P3-CNRS (France).

Data Availability Statement The data used in this paper were collected before February 2022.

Code Availability Statement Code/software will be made available on reasonable request. [Author's comment: The code/software generated during and/or analysed during the current study is available from the corresponding author on reasonable request.]

References

1. E.V. Shuryak, Quantum chromodynamics and the theory of superdense matter. Phys. Rep. **61**, 71–158 (1980). https://doi.org/10.1016/0370-1573(80)90105-2
2. J. Letessier, J. Rafelski, *Hadrons and Quark-Gluon Plasma* (Oxford University Press, Oxford, 2002). https://doi.org/10.1017/9781009290753
3. M. Gazdzicki, M.I. Gorenstein, On the early stage of nucleus–nucleus collisions. Acta Phys. Pol. B **30**, 2705 (1999). arXiv:hep-ph/9803462
4. M. Gazdzicki, Z. Fodor, G. Vesztergombi, [NA49-future Collaboration Collab.], Study of Hadron Production in Hadron-Nucleus and Nucleus-Nucleus Collisions at the CERN SPS, Tech. Rep. CERN-SPSC-2006-034. SPSC-P-330, CERN, Geneva (2006). https://cds.cern.ch/record/995681. Revised version submitted on 2006-11-06 12:38:20
5. A. Acharya et al., [NA61/SHINE Collab.], K^0_S meson production in inelastic p+p interactions at 158 GeV/c beam momentum measured by NA61/SHINE at the CERN SPS. Eur. Phys. J. C **82**(1), 96 (2022). https://doi.org/10.1140/epjc/s10052-021-09976-y. arXiv:2106.07535 [hep-ex]
6. A. Aduszkiewicz et al., [NA61/SHINE Collab.], Measurements of $\pi^\pm$, $K^\pm$, p and $\bar{p}$ spectra in proton-proton interactions at 20, 31, 40, 80 and 158 GeV/c with the NA61/SHINE spectrometer at the CERN SPS. Eur. Phys. J. C **77**(10), 671 (2017). https://doi.org/10.1140/epjc/s10052-017-5260-4. arXiv:1705.02467 [nucl-ex]
7. N. Abgrall et al., [NA61 Collab.], NA61/SHINE facility at the CERN SPS: beams and detector system. JINST **9**, P06005 (2014). https://doi.org/10.1088/1748-0221/9/06/P06005. arXiv:1401.4699 [physics.ins-det]
8. N. Abgrall et al., [NA61/SHINE Collab.], Measurement of negatively charged pion spectra in inelastic p+p interactions at p_{lab} = 20, 31, 40, 80 and 158 GeV/c. Eur. Phys. J. C **74**(3), 2794 (2014). https://doi.org/10.1140/epjc/s10052-014-2794-6. arXiv:1310.2417 [hep-ex]
9. A. Aduszkiewicz et al., [NA61/SHINE Collab.], Multiplicity and transverse momentum fluctuations in inelastic proton–proton interactions at the CERN Super Proton Synchrotron. Eur. Phys. J. C **76**(11), 635 (2016). https://doi.org/10.1140/epjc/s10052-016-4450-9. arXiv:1510.00163 [hep-ex]
10. A.P.C. Bovet, R. Maleyran, M. Placidi, The cedar (cerenkov differential counters with achromatic ring focus) project. IEEE Trans. Nucl. Sci. **25**(1), 572–576 (1978)
11. C. Strabel, Evaluation of Particle Yields in 30 GeV Proton-Carbon Inelastic Interactions for Estimating the T2K Neutrino Flux. Ph.D. thesis, Frankfurt U. (2011). https://doi.org/10.3929/ethz-a-006511036
12. A. Aduszkiewicz et al., [NA61/SHINE Collab.], Two-particle correlations in azimuthal angle and pseudorapidity in inelastic p + p interactions at the CERN Super Proton Synchrotron. Eur. Phys. J. C **77**(2), 59 (2017). https://doi.org/10.1140/epjc/s10052-017-4599-x. arXiv:1610.00482 [nucl-ex]
13. N. Abgrall, [NA61 Collab.], Calibration and Analysis of the 2007 Data, tech. rep., CERN, Geneva (2008). https://cds.cern.ch/record/1113279
14. N. Abgrall et al., [NA61/SHINE Collab.], Measurements of cross sections and charged pion spectra in proton–carbon interactions at 31 GeV/c. Phys. Rev. C **84**, 034604 (2011). https://doi.org/10.1103/PhysRevC.84.034604. arXiv:1102.0983 [hep-ex]
15. A. Aduszkiewicz et al., [NA61/SHINE Collab.], Production of Λ -hyperons in inelastic p+p interactions at 158 GeV/c. Eur. Phys. J. C **76**(4), 198 (2016). https://doi.org/10.1140/epjc/s10052-016-4003-2. arXiv:1510.03720 [hep-ex]
16. M. Tanabashi et al., [Particle Data Group Collab.], Review of particle physics. Phys. Rev. D **98**(3), 030001 (2018) . https://doi.org/10.1103/PhysRevD.98.030001
17. A. Aduszkiewicz et al., [NA61/SHINE Collab.], $K^*(892)^0$ meson production in inelastic p+p interactions at 158 GeV/c beam momentum measured by NA61/SHINE at the CERN SPS. Eur. Phys. J. C **80**(5), 460 (2020). https://doi.org/10.1140/epjc/s10052-020-7955-1. arXiv:2001.05370 [nucl-ex]
18. J. Podolanski, R. Armenteros III., Analysis of V-events. Lond. Edinb. Dublin Philos. Mag. J. Sci. **45**(360), 13–30 (1954). https://doi.org/10.1080/14786440108520416
19. K. Werner, F.M. Liu, T. Pierog, Parton ladder splitting and the rapidity dependence of transverse momentum spectra in deuteron-gold collisions at RHIC. Phys. Rev. C **74** (2006). https://doi.org/10.1103/PhysRevC.74.044902

20. T. Pierog, K. Werner, EPOS model and ultra high energy cosmic rays. Nucl. Phys. B Proc. **196**, 102–105 (2009). https://doi.org/10.1016/j.nuclphysbps.2009.09.017
21. R. Brun et al., GEANT: Detector Description and Simulation Tool; Oct 1994. CERN, Geneva (1993). https://doi.org/10.17181/CERN.MUHF.DMJ1. https://cds.cern.ch/record/1082634. Long Writeup W5013
22. J. Mohs, S. Ryu, H. Elfner, Particle production via strings and baryon stopping within a hadronic transport approach. J. Phys. G **47**(6), 065101 (2020). https://doi.org/10.1088/1361-6471/ab7bd1. arXiv:1909.05586 [nucl-th]
23. W. Cassing, E.L. Bratkovskaya, Parton transport and hadronization from the dynamical quasiparticle point of view. Phys. Rev. C **78**, 034919 (2008). https://doi.org/10.1103/PhysRevC.78.034919. arXiv:0808.0022 [hep-ph]
24. W. Cassing, E.L. Bratkovskaya, Parton-hadron-string dynamics: an off-shell transport approach for relativistic energies. Nucl. Phys. A **831**, 215–242 (2009). https://doi.org/10.1016/j.nuclphysa.2009.09.007. arXiv:0907.5331 [nucl-th]
25. V. Blobel et al., Multiplicities, topological cross sections, and single particle inclusive distributions from pp interactions at 12 and 24 GeV/c. Nucl. Phys. B **69**, 454–492 (1974). https://doi.org/10.1016/0550-3213(74)90449-0
26. V.V. Ammosov et al., Neutral strange particle production in p p interactions at 69-GeV/c. Nucl. Phys. B **115**, 269–286 (1976). https://doi.org/10.1016/0550-3213(76)90257-1
27. H. Adhikary, [NA61 Collab.], Excess of charged over neutral K meson production in high-energy collisions of atomic nuclei. tech. rep., CERN, Geneva (2023). arXiv:2312.06572. https://cds.cern.ch/record/2883229. 18 pages, 6 figures
28. J. Stepaniak, D. Pszczel, On the relation between K_s^0 and charged kaon yields in proton–proton collisions. Eur. Phys. J. C **83**(10), 928 (2023). https://doi.org/10.1140/epjc/s10052-023-12108-3. arXiv:2305.03872 [hep-ph]
29. L. Gatignon, Design and Tuning of Secondary Beamlines in the CERN North and East Areas. https://cds.cern.ch/record/2730780
30. R.I. Louttit, T.W. Morris, D.C. Rahm, R.R. Rau, A.M. Thorndike, W.J. Willis, R.M. Lea, Production of strange particles in $p - p$ collisions at 2.85 GeV. Phys. Rev. **123**, 1465–1471 (1961). https://doi.org/10.1103/PhysRev.123.1465
31. G. Alexander et al., Proton–proton interactions at 5.5 GeV/c. Phys. Rev. **154**, 1284–1304 (1967). https://doi.org/10.1103/PhysRev.154.1284
32. M. Firebaugh et al., Strange-particle production in 8-GeV/c proton–proton interactions. Review **172**, 1354–1369 (1968). https://doi.org/10.1103/PhysRev.172.1354Phys
33. H. Fesefeldt et al., Strangeness-transfer distributions in proton–proton collisions at 12 and 24 GeV/c. Nucl. Phys. B **147**, 317–335 (1979). https://doi.org/10.1016/0550-3213(79)90318-3
34. M.Y. Bogolyubsky et al., Study of neutral strange particle production in pp interactions at 32-GeV/c and comparison with $\bar{p}p$ data. Sov. J. Nucl. Phys. **50**, 424 (1989)
35. M. Alston-Garnjost et al., Neutral particle production in $\pi^+ p$ and pp collisions at 100 GeV/c. Phys. Rev. Lett. **35**, 142–145 (1975). https://doi.org/10.1103/PhysRevLett.35.142
36. J.W. Chapman et al., Production of γ, Λ^0, K_S^0 and $\bar{\Lambda}^0$ in pp collisions at 102 GeV/c. Phys. Lett. B **47**, 465–468 (1973). https://doi.org/10.1016/0370-2693(73)90116-0
37. D. Brick et al., Inclusive production of neutral strange particles by 147-GeV/c Pi+ K+ p interactions in hydrogen. Nucl. Phys. B **164** (1980). https://doi.org/10.1016/0550-3213(80)90499-X
38. K. Jaeger et al., Characteristics of V^0 and γ production in pp interactions at 205 GeV/c. Phys. Rev. D **11**, 2405–2425 (1975). https://doi.org/10.1103/PhysRevD.11.2405
39. A. Sheng et al., pp interactions at 300 GeV/c: γ and neutral-strange-particle production. Phys. Rev. D **11**, 1733–1742 (1975). https://doi.org/10.1103/PhysRevD.11.1733
40. F. LoPinto et al., Inclusive K^0, Λ^0, $K^{*\pm}(890)$, and $\Sigma^{*\pm}(1385)$ production in pp collisions at 300 GeV/c. Phys. Rev. D **22**, 573–581 (1980). https://doi.org/10.1103/PhysRevD.22.573
41. M. Asai, et al., [EHS-RCBC, Bombay-CERN-Genoa-Innsbruck-Japan-Madrid-Mons-Rutgers-Serpukhov-Tennessee-Vienna Collab.], Inclusive K_S^0, Λ and $\bar{\Lambda}$ Production in 360-GeV/cpp Interactions Using the European Hybrid Spectrometer. Z. Phys. C **27**, 11 (1985). https://doi.org/10.1007/BF01642475
42. R.D. Kass et al., Charged- and neutral-particle production from 400-GeV/c pp collisions. Phys. Rev. D **20**, 605–614 (1979). https://doi.org/10.1103/PhysRevD.20.605
43. H. Kichimi et al., Inclusive study of strange-particle production in pp interactions at 405 GeV/c. Phys. Rev. D **20**, 37–52 (1979). https://doi.org/10.1103/PhysRevD.20.37